# OBJECT-AWARE CONDITIONAL ALIGNMENT FOR CROSS-DOMAIN COUNTING

**Anonymous authors**
Paper under double-blind review

## ABSTRACT

Object counting is an important task in computer vision with many real-world applications. In practical settings, factors such as lighting conditions and object density can vary dramatically, leading to distribution shifts then causing inaccurate counting. We found that existing domain adaptation (DA) methods cannot be directly applied to the counting task, as they usually assume changes across different domains are task-irrelevant and focus on utilizing domain-invariant features for prediction. However, in object counting tasks, changes in object density which could happen across domains are task-relevant and cannot be ignored. Therefore, applying existing DA methods to the counting task can ignore the information about density changes, resulting in unreliable counting. To address this limitation, we propose the Binary Alignment Network (BiAN). Unlike traditional DA methods that align distributions of entire image representations, BiAN segments objects of interest and aligns the distributions of the object-specific features across domains. This targeted alignment allows us to disregard irrelevant features, such as lighting conditions while preserving essential information about changes in object density. We theoretically demonstrate that BiAN achieves superior adaptability in counting tasks by introducing conditional alignment—aligning features conditioned on the presence of objects. Extensive experiments on two distinct counting tasks and eight dataset combinations show that BiAN outperforms state-of-the-art methods.

## 1 INTRODUCTION

Object counting is an important task in computer vision with a wide range of real-world applications, including crowd monitoring, traffic analysis, and biomedical imaging. Accurate counting of objects within images or video frames is crucial for decision-making processes in various industries and research domains (He et al., 2021). However, in practical settings, factors such as lighting conditions, object density, and background complexity can vary dramatically across different environments. These variations lead to distribution shifts between training data (source domain) and deployment scenarios (target domain), posing significant challenges for object counting models (Wang et al., 2019b).

To address distribution shifts, domain adaptation (DA) methods have been widely explored in machine learning. These methods aim to improve the generalization capabilities of models by aligning the feature distributions between source and target domains (Singhal et al., 2023). In tasks like image classification and semantic segmentation, DA methods generally assume that domain shifts are task-irrelevant, meaning the shifts do not affect the core features necessary for accurate predictions (Kong et al., 2022; Xie et al., 2023b; Bousmalis et al., 2016). By focusing on learning domain-invariant features, these methods strive to maintain performance across different domains.

However, this assumption does not hold in the context of object counting. Changes in object density across domains are inherently task-relevant, as the primary goal is to accurately estimate the number of objects

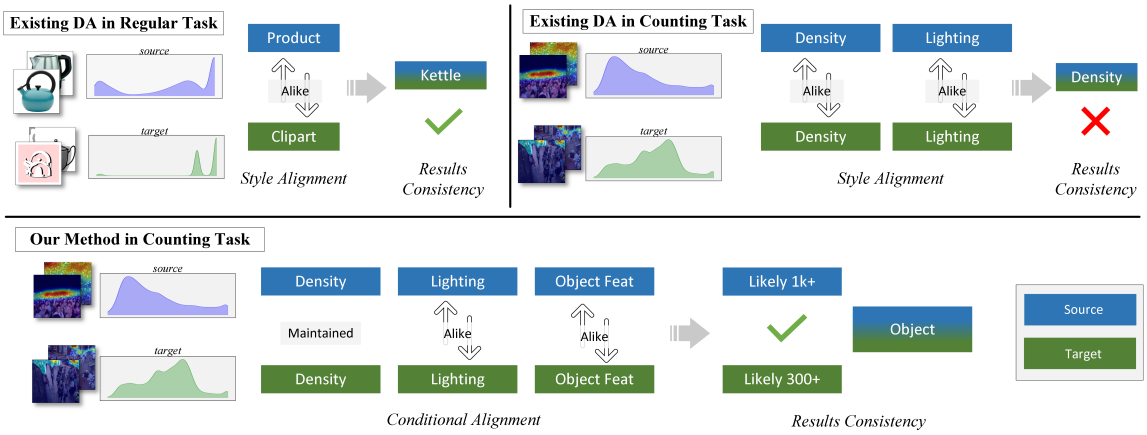


Figure 1: Comparison between existing domain adaptation (DA) methods and our approach. It shows that the general DA methods treat task-relevant factors as features that need to be directly aligned. The aligned distribution of density leads to consistent density estimation across domains. However, the consistent density does not match the real density in the samples. In our method, we only align the distributions of features belonging to objects of interest, so that the inter-object information can be preserved.

present (Li et al., 2019; Han et al., 2023). As shown in Figure 1, traditional DA methods that ignore these density variations may inadvertently discard crucial information, leading to unreliable counting performance on the target domain. The misalignment arises because these methods treat all domain shifts uniformly, failing to distinguish between task-relevant and task-irrelevant variations. The existing domain adaptive counting methods like CODA notice the issue of dynamic density (Li et al., 2019). However, they still consider the density feature as domain invariant and then struggle with aligning its distribution, which is in conflict with the assumption.

To tickle this limitation, we propose the Binary Alignment Network (BiAN), a novel approach designed specifically for domain adaptation in object counting tasks. Figure 1 shows the sketch of our proposed method. Instead of aligning the distributions of entire image representations, BiAN focuses on segmenting objects of interest and aligning the distributions of their features across domains. By isolating the features within the objects, our method effectively filters out task-irrelevant variations such as lighting conditions and background noise, while preserving essential information about object density changes. This targeted alignment ensures that the model remains sensitive to variations that directly impact the counting task.

We further provide a theoretical framework demonstrating that BiAN achieves superior adaptability by introducing conditional alignment—aligning features conditioned on the presence of objects. This approach allows the model to account for density variations between domains more effectively than traditional methods. By conditioning on object presence, BiAN maintains sensitivity to the number and arrangement of objects, which are critical factors in accurate counting.

Our main contributions are summarized as follows:

- We highlight the shortcomings of existing domain adaptation techniques when applied to object counting tasks. Specifically, the existing DA methods contempt the dynamic density across scenes as the task-relevant factor, violating the DA assumption. The aligned density distribution causes source-consistency density estimation, leading to decay in counting performance.

- We introduce BiAN, which segments objects of interest and aligns their features across domains conditionally. Within BiAN, the conditional alignment is proposed for aligning the distribution of object feature and background and preserving inter-object contextual information. The additional consistency mechanism further guarantees the crucial density information by constraining the conditional aligned distribution consistent with the distribution of the entire sample.
- We provide a theoretical demonstration of how conditional alignment enhances domain adaptability in counting tasks. The analysis demonstrates that aligning the distribution of specific conditions is beneficial to overall alignment performance. It also emphasizes the importance of maintaining consistency between condition-level distribution and sample-level distribution.
- We conduct comprehensive experiments on multiple counting scenarios with different density variations. The results show that BiAN significantly outperforms existing methods in terms of counting accuracy.

In the following sections, we review related work, detail the methodology of BiAN, present our theoretical findings, and discuss the experimental results that demonstrate the advantages of our approach.

## 2 Related Work

### 2.1 Object Counting

Object counting is a fundamental task in computer vision, with applications in various fields, such as crowd monitoring, cell counting, and traffic analysis (Loy et al., 2013). Traditional counting methods rely on supervised learning, which requires a large amount of annotated data (Jiang et al., 2021; Liu et al., 2021; Gao et al., 2021). Recent advances in deep learning have significantly improved the performance of counting models. For instance, Kernel-based Density Map Generation (KDMG) (Wan et al., 2022) employs a kernel-based density map to estimate the object count. SAU-Net (Guo et al., 2022) combines the advantages of SANet and U-Net to achieve high counting accuracy. STEERER (Han et al., 2023) cumulatively selects and inherits discriminative features to resolve scale variations. Despite the remarkable performance of these models, they are limited by the requirement of large amounts of annotated data when encountering domain variety. Therefore, GAN-based UDA counting methods have been proposed, such as Counting Object via scale-aware adversarial Density Adaptation (CODA) (Li et al., 2019), devised to address distinct object scale and density distributions. Additionally, SSIM Embedding Cycle GAN (SECycle) (Wang et al., 2019b) has emerged as a potent solution for counting in natural crowd scenes by synthesizing target-like images. To amplify the model's adaptability across intricate scenarios, the novel Latent Domain Generation (LDG) (Zhang et al., 2023) method has been introduced, generating the latent domain to learn the distribution from domains. The advanced research adopts the latest approaches in other fields, such as SaKnD (Xie et al., 2023a) which utilizing diffusion modules to enhance generalizability and CrowdGraph (Zhang et al., 2024a) which proposed an algorithm via pure graph neural network. To the best of our knowledge, there remains a research gap in discriminate migration for preserving task-relevant information across domains.

### 2.2 Domain Adaptation

Domain adaptation (Cai et al., 2019; Courty et al., 2017; Deng et al., 2019; Tzeng et al., 2017; Wang et al., 2019a; Xu et al., 2019; Zhang et al., 2017; 2020; Mao et al., 2024; Stojanov et al., 2024; Wu et al., 2022; Eastwood et al., 2022; Tong et al., 2022; Kirchmeyer et al., 2022; Zhu et al., 2022; Xu et al., 2022; Roelofs et al., 2022; Kong et al., 2022; Jiang et al., 2022; Liu et al., 2022; Zhang et al., 2024b) has become a focal point in recent computer vision and machine learning research. Among the various approaches, invariant representation learning, introduced by (Ganin & Lempitsky, 2015), stands out as a direct and increasingly popular method. The goal of invariant representation learning is to identify domain-invariant features, that can reconstruct the original data for predicting label (Bousmalis et al., 2016). Historically, it was assumed

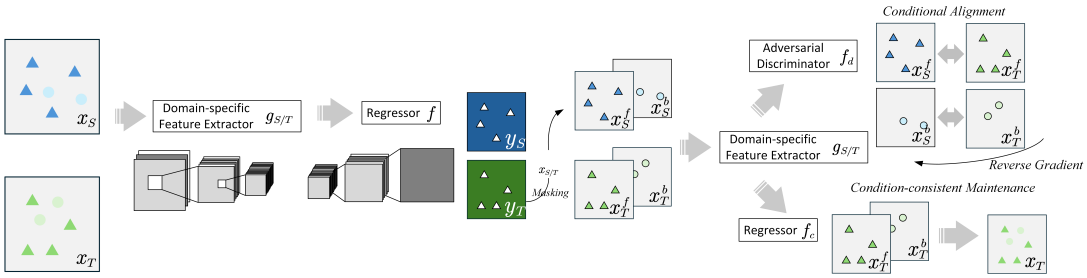


Figure 2: Overview of our proposed BiAN framework. $g_s$ and $g_t$ are domain-specific feature extractors for source and target domain. $f_d$ is the domain discriminator for aligning. $f$ is the regressor for generating target density map. $f_c$ is the regressor for generating conditional density map with shared weights with $f$.

that the distribution of labels remains consistent across different domains. Based on this assumption, cluster-based and kernel-based methods have been developed to approximate the joint label distribution (Long et al., 2018; Xie et al., 2018a; Shu et al., 2018). In general, it is hard to guarantee that domain-invariant features capture the discriminative information needed for label prediction in a setting of single source domain (Kong et al., 2022). Multi-source adaptation offers potential solutions (Xu et al., 2018; Peng et al., 2019; Park & Wan Lee, 2021; Li et al., 2021; Wang et al., 2020), where theoretical studies have demonstrated that latent variables can be identified from a sufficient number of source domains using independent component analysis. However, the existing methods are limited by the assumption that the domain shifts are task-irrelevant. In contrast, our proposed BiAN focuses on aligning the distribution of object-specific features across domains, which allows us to disregard irrelevant features while preserving essential information about object density changes.

## 3 METHODS

In this section, we formally propose the Binary Alignment Network (BiAN) for cross-domain counting tasks. We first describe the conditional alignment process in Figure 2 and discuss how we can mitigate the domain shift of object features while preserving crucial density information. We introduce conditional alignment and consistency mechanisms in Section 3.2 and Section 3.3. The training process of BiAN is shown as Appendix A.2. We also provide a theoretical analysis of conditional alignment in Section 3.5, demonstrating how BiAN achieves superior adaptability in counting tasks.

### 3.1 PRELIMINARY STUDY

In this section, we review the preliminary knowledge of cross-domain counting task. The objective of cross-domain counting is to train a network $\mathcal{N}$ that transfers the counting-relevant knowledge from source domain $D_s$ to $D_t$ with minimum joint decision error $\epsilon_U$. The network $\mathcal{N}$ process can be formulated as a Markov chain that $\mathcal{X} \xrightarrow{g} \mathcal{Z} \xrightarrow{f} \mathcal{Y}$. The error $\epsilon_U$ can be represented $\epsilon_U = \epsilon_{D_{s'}}(h) + \epsilon_{D_{t'}}(h)$, where $\epsilon_{D_{s'}}(h)$ and $\epsilon_{D_{t'}}(h)$ indicate the decision error on the transferred domains. The decision error $\epsilon$ can be represented as $\epsilon(h, f_i)$, where $h$ for hypothesis and $f_i^L$ for labeling function on the transferred domain (Zhao et al., 2019). The general DA interacts with domain-variant and domain-invariant features, which are $z_{var}$ and $z_{inv}$ respectively. The fundamental assumption is that $z_{var}$ does not influence the label $y$ (Kong et al., 2022). Specifically, the sketch of general DA can be represented as first identifying $z_{inv}$ and $z_{var}$, then processing $z_{inv}$ for recognition and migrating $z_{var}$ to the unified domain. Different from general DA approaches, the task of counting across domains introduces the concept of task-relevant factors $z_{task}$, which is domain-

variant but relevant to the results. Therefore, preserving $z_{task}$ is required for the stable counting adaptation process. In BiAN, we treat $z_{task}$ as contextual information between condition subsets and preserving it via conditional alignment and encourage network $\mathcal{N}_{BiAN}$ to maintain $z_{task}$. The definition of the elements can be represented as:

**Definition 1.** *Given domain-variant probability distributions $D_s$ and $D_t$ over an independent variable $\mathcal{X}$, which are $\mathcal{X}_s$ and $\mathcal{X}_t$ respectively. Let $g_s$ and $g_t$ be two reflections to project $\mathcal{X}_s$ and $\mathcal{X}_t$ to an overlapped feature domain $\mathcal{Z}_U$. The unified domain $\mathcal{Z}_U$ and label space $\mathcal{Y}$ can be represented as:*

$$\begin{aligned} &\mathcal{Z}_s = g_s\left(\mathcal{X}_s\right),\ \mathcal{Z}_t = g_t\left(\mathcal{X}_t\right), \\ &\mathcal{Z}_U = \mathcal{Z}_s \cup \mathcal{Z}_t, \mathcal{Z}_s \cap \mathcal{Z}_t \neq \varnothing. \\ &\mathcal{Y}_s = f_s\left(\mathcal{Z}_s\right),\ \mathcal{Y}_t = f_t\left(\mathcal{Z}_t\right). \end{aligned}$$

### 3.2 Condition Alignment

Within the framework of BiAN, we design conditional alignment with the following alignment strategy. It aims to independently align the conditional subsets $D_s^c = \{x_s^i, x_s^i \subseteq x^i \in D_s\}$ and $D_t^c = \{x_t^i, x_t^i \subseteq x^i \in D_t\}$ to maintain the distribution of contextual density information between conditions. It is straight to segment the entire feature into two condition subsets, which are objects of interest and background. In BiAN, there are two subsets to be aligned with minimal joint error.

In the following step, conditional alignment is adopted to operate the alignment depending on the segmentation results of images. The entire image $x$ is sent to recognize the relation between conditions. Then, the condition relation segments the entire image $x$ into object parts $x^f$ and background $x^b$. Lastly, these two subset features $z^f$ and $z^b$ can be obtained by feature extractor $g_{s/t}$ for conditional alignment. Specifically, the feature can be obtained by $z = g_{s/t}(x)$. Then, the object label prediction $\hat{y}$ can be obtained by $\hat{y} = f(z)$. If $(x, y) \in D_s$, we can further align the distribution convergence of $f(z)$ and $y$, which can be represented as:

$$g^* = \arg\min_g \mathcal{L}\left(f\left(g\left(\mathcal{X}_s\right)\right), \mathcal{Y}_s\right). \tag{1}$$

If $(x, y) \in D_t$, we still can obtain the pseudo $\hat{y}_t$ as the position-condition feature for the target domain $D_t$. After that point, $\hat{y}$ is applied as a mask indicator on $x$, then the image is divided into conditional subsets. Specifically, the mask can be generated from the predicted points of objects in $\hat{y}$ by extending range. The condition partitions $x^i$ can be represented as: $x = \bigcup_{i \in [f,b]} x^i \ \left(x^i \cap x^j = \varnothing, i \neq j\right)$. Then, the conditional partitions are sent to $g_i$ to obtain the conditional features $z_f$ and $z_b$. After that, we operate the alignment within the condition subset for all conditions included in the condition set $\mathcal{C}$. It means that every single alignment operation is only applied on $\bigcup_i z_i$. The operation can be represented as:

$$f^* = \arg\min_f d_{\mathcal{C}}\left(f\left(\mathcal{X}_s\right), f\left(\mathcal{X}_t\right)\right). \tag{2}$$

We suppose the combination of $f^*$ and $g^*$ are able to conditionally align the domain $D_s$ and $D_t$. According to Theorem 4, BiAN can achieve a lower joint decision error without being impacted by the conditional shift.

As for the specific model, we adopt SAU-Net (Guo et al., 2022) as the backbone of BiAN and modify it to make it capable of UDA counting tasks. Specifically, the components $g_{s/t}$ and $f$ source from the encoder and decoder in SAU-Net. To implement the aligning operation, the discriminator in DANN (Ganin & Lempitsky, 2015) is adopted as $f_d$ to fuse the domains by reversing the gradient during backpropagation.

### 3.3 CONDITION-CONSISTENT MECHANISM

In this section, we formally propose the Condition-consistent Mechanism (CM) to refine the pseudo labels in the target domain. Since the mask of the target domain is obtained via pseudo-labeling, it is essential to introduce CM to further enhance the self-supervised process. We suppose that partial distribution overlaps exist between domains. Thus, BiAN can learn to recognize part of target samples by leveraging knowledge from the source domain. After learning the distribution of objects, the network can directly segment the background and then learn the background feature. The obtained background feature distribution contrastively helps to learn about object features. Therefore, it is vital to maintain contextual information between condition subsets, which is our motivation for designing CM. In the conditional alignment process, the partitions sharing the same condition are sent to $g_{s/t}$ and $f$. Then, the results of $f(z^i)$ are expected to maintain as $y^i \in y$. Moreover, because $x^i \cap x^j = \varnothing$ when $i \neq j$, it is supposed that $y = concat\left(y^i\right)$, where $i \in f, b$. Specifically, we design a regressor $f_c$ which shares weights with $f$. For the evaluation of result consistency, we design a consistency loss, which can be represented as:

$$\hat{y}' = concat\left(f_c \circ g_t\left(x_t^f\right), f_c \circ g_t\left(x_t^b\right)\right), \tag{3}$$

$$\mathcal{L}_{CM} = \mathcal{L}\left(\hat{y}', f_t \circ g_t\left(x_t\right)\right), \tag{4}$$

where $R$ is the aforementioned regressor. We apply $MSE$ loss as $\mathcal{L}$. CM helps $F_t$ to transform different partial image information without annotation through minimizing $\mathcal{L}_{CM}$.

### 3.4 LOSS FUNCTIONS

In this section, we describe the loss function applied for training BiAN. The loss function can be divided into loss of source domain and loss of target domain. It can be represented as:

$$\mathcal{L} = \mathcal{L}_{source} + \mathcal{L}_{target} + \alpha\mathcal{L}_{CM}, \tag{5}$$

$$\mathcal{L}_{source} = \frac{\mathcal{L}_p\left(\hat{y}_s, y_s\right) + \mathcal{L}_p\left(\hat{y}_s^f, y_s\right) + \mathcal{L}_p\left(\hat{y}_s^b, \mathbf{0}\right)}{\mathcal{L}_d\left(\hat{c}_s^f, y_s^d\right) + \mathcal{L}_d\left(\hat{c}_s^b, y_s^d\right)}, \tag{6}$$

$$\mathcal{L}_{target} = \frac{\mathcal{L}_p\left(\hat{y}_t^b, \mathbf{0}\right)}{\mathcal{L}_d\left(\hat{c}_t^f, y_t^d\right) + \mathcal{L}_d\left(\hat{c}_t^b, y_t^d\right)}, \tag{7}$$

where $\hat{c}_{s/t}^* = \{0, 1\}$ is the output of $f_d(z_{s/t}^*)$, presenting the predication of which domain sample belonging to. And $y^d$ denotes the domain label of the sample. $\mathcal{L}_p$ is $MSE$ loss, $\mathcal{L}_d$ is applied reversed $NLL$ loss, maintaining $L_s$ positive. $\mathbf{0}$ in $\mathcal{L}_p$ presents background. The coefficient $\alpha$ presents the weight of $CM$ to balance the orders of magnitude with the rest of the loss elements. The employed $\mathcal{L}_d$ and $\mathcal{L}_p$ loss can be represented as:

$$\mathcal{L}_d\left(\hat{c}_i, y_i^d\right) = \frac{1}{N}\sum_{i=1}^{N} y_i^d \log(\hat{c}_i) + (1 - y_i^d)\log(1 - \hat{c}_i), \tag{8}$$

$$\mathcal{L}_p\left(\hat{y}_i, y_i\right) = \frac{1}{N}\sum_{i=1}^{N}(y_i - \hat{y}_i)^2, \tag{9}$$

where $y_i^d$ indicates the domain of the sample, $\hat{c}_i$ denotes the prediction of sample domain. $y_i$ is the ground-truth counting map of the sample, $\hat{y}_i$ is the prediction of counting map. $N$ indicates the amount of samples.

### 3.5 THEORETICAL ANALYSIS

In this section, we prove that the proposed BiAN can achieve a lower bound of joint decision error on both domains. First, the adaptation task can be represented as follows. For the source domain $D_s$ and the target domain $D_t$, our goal is searching the optimal decision hypothesis function $h^* = g \circ f$ to simultaneously reach the least joint decision loss $\lambda$ in all transferred domains. However, it has been proved that the unconditional alignment leads to the significant constraint of lowering the joint decision error, causing the burden of further increasing the adaptability of models (Zhao et al., 2019). Specifically, the goal of unconditional alignment can be represented as $\arg\min_h |d_{\mathcal{H}\Delta\mathcal{H}}(h(D), h(D'))|$. Zhao's paper (Zhao et al., 2019) has provided a comprehensive deduction that under the significantly large marginal difference between label space of domains, the joint decision error $|\epsilon_D(h^*, f) + \epsilon_{D'}(h^*, f')|$ has the lower bound as $|d_{JS}(\mathcal{Y}, \mathcal{Y}') - d_{JS}(D, D')|$. The constraint still holds while adopting the sophisticated unconditional transferring function. Therefore, we introduce a theorem of conditional adaptation and prove that it helps the adaptation model achieve lower joint decision error. We first introduce the definition of variables and symbols. Then, we describe our proposed theorem and provide the corresponding proof. Note that we provide the key definitions. The rest of symbols and variables in this paper follow the definitions in Ben-David's paper (Ben-David et al., 2009).

**Definition 2** (Divergence Measurement)**.** *Given a hypothesis function $h$ and two domains $D$ and $D'$. Let $I$ be the identifying function. The divergence measurement between $D$ and $D'$ can be represented as:*

$$d_{JS}(D, D') = \frac{1}{2} d_{\mathcal{H}\Delta\mathcal{H}}\left(D, \frac{(D + D')}{2}\right) + \frac{1}{2} d_{\mathcal{H}\Delta\mathcal{H}}\left(D', \frac{(D + D')}{2}\right),$$

*where $d_{\mathcal{H}\Delta\mathcal{H}}(D, D') = 2sup|Pr_D[I(h)] - Pr_{D'}[I(h)]|$.*

**Definition 3** (Conditional Subset)**.** *Given a domain probability distributions $D$ over $\mathcal{X}$. Let $\mathcal{C} = \{c_1, c_2, c_3, \ldots, c_k\}$ be a condition set of $D$. The conditional subset of $D$ is*

$$D = \bigcup_{i=1}^{k} D_i^c, i \neq j, D_i^c \cap D_j^c = \varnothing.$$

Specially, the condition set $\mathcal{C}$ denotes the attributes of partitions within samples (e.g. background and foreground in counting sample).

**Definition 4** (Conditional Divergence)**.** *Given $D$ and $D'$ shared the same condition set $\mathcal{C}$, the conditional divergence can be defined as:*

$$d_{\mathcal{C}}(D, D') = \sum_{i \in [1,k]} d_{JS}(D_i^c, D_i'^c).$$

*If $d_{\mathcal{C}}(D, D') = 0$, $D$ and $D'$ are supposed as conditional aligned on condition $\mathcal{C}$.*

**Theorem 1** (Joint Error Lower Bound)**.** *Based on the theorem proposed in (Zhao et al., 2019), combining the definition of the joint error $\epsilon_U = \epsilon_{\mathcal{Z}}(h) + \epsilon_{\mathcal{Z}'}(h)$ and the unified feature space $Z_U$, the corresponding lower bound can be rewritten as:*

$$\epsilon_U \geqslant \frac{1}{2}\left(d_{JS}(\mathcal{Y}, \mathcal{Y}') - d_{JS}(\mathcal{Z}, \mathcal{Z}')\right)^2.$$

**Lemma 2.** *Assume the label space $\mathcal{Y}$ of $D$ and $D'$ is discrete. If consider treat the label set as the condition set $\mathcal{C}$, the relation of $\mathcal{Y}$ and $\mathcal{Y}'$ can be presented as:*

$$d_{\mathcal{C}}(\mathcal{Y}, \mathcal{Y}') = 0.$$

According to the definition of $d_{JS}$ and $\mathcal{Y}, \mathcal{Y}'$, the labeling function is always consistent. So that $\mathcal{Y}, \mathcal{Y}'$ are always conditionally aligned when treating the label set as the condition set. Details of the proof can be found in Appendix A.3.

Table 1: Counting MAE and MSE on JHU-Crowd++ with labels "Stadium"(SD), "Street"(SR), "Snow"(SN) and "Fog/Haze"(FH). The best are highlighted in bold. DA: Domain Adaptation for short. DG: Domain Generalization for short.

| Method | DA | DG | SD→SR | | SR→SD | | SN→FH | | FH→SN | |
|---|---|---|---|---|---|---|---|---|---|---|
| | | | MAE ↓ | MSE ↓ | MAE ↓ | MSE ↓ | MAE ↓ | MSE ↓ | MAE ↓ | MSE ↓ |
| BL (Ma et al., 2019) | ✗ | ✗ | 42.1 | 79 | 262.7 | 1063.9 | 48.1 | 129.5 | 343.8 | 770.5 |
| MAN (Lin et al., 2022) | ✗ | ✗ | 45.1 | 79 | 246.1 | 950.8 | 38.1 | 68 | 445 | 979.3 |
| DAOT (Zhu et al., 2023) | ✔ | ✗ | 45.3 | 88 | 278.7 | 1624.3 | 42.3 | 73 | 151.6 | 273.9 |
| IBN (Pan et al., 2018) | ✗ | ✔ | 92.2 | 178 | 318.1 | 1420.4 | 109.7 | 267.7 | 491.8 | 1110.4 |
| SW (Pan et al., 2019) | ✗ | ✔ | 110.3 | 202.4 | 312.6 | 1072.4 | 131.5 | 306.6 | 381.3 | 825 |
| ISW (Choi et al., 2021) | ✗ | ✔ | 108.1 | 212.4 | 385.9 | 1464.8 | 151.6 | 365.7 | 276.6 | 439.8 |
| DCCUS (Du et al., 2023) | ✗ | ✔ | 90.4 | 194.1 | 258.1 | 1005.9 | 54.5 | 125.8 | 399.7 | 945 |
| MPCount (Peng & Chan, 2024) | ✗ | ✔ | 37.4 | 70.1 | 218.6 | 935.9 | 31.3 | **55** | 216.3 | 421.4 |
| BiAN (Ours) | ✔ | ✗ | **28.9** | **39.6** | **115.7** | **145.1** | **23.6** | 68.4 | **120.2** | **150.7** |

**Lemma 3.** *Given $D$ and $D'$ shared the discrete label space $\mathcal{Y}$ and set as the condition set $\mathcal{C}$, if $D_i^c \cap D' = D'^c$ the relation of the conditional subset of $D$ and the universal set of $D'$ can be presented as:*

$$d_{JS}\left(\mathcal{Y}_i^c, '\right) = d_{JS}\left(D_i^c, D_i'^c\right).$$

According to the definition of $d_{JS}$ and the definition 4, the proof is obvious. The proof can be found in Appendix A.4.

**Theorem 4** (Conditional Alignment)**.** *Given $D$ and $D'$ shared the discrete label space $\mathcal{Y}$ and set as the condition set $\mathcal{C}$, if $D$ and $D'$ is conditional aligned on label space $\mathcal{Y}$, then $d_{JS}\left(D, D'\right) = d_{JS}\left(\mathcal{Y}, \mathcal{Y}'\right)$.*

We present the proof in Appendix A.5. The deduction above shows that the joint error is bounded by the domain shift in both features and labels. Under reasonable assumptions, our proposed theorem presents a feasible approach to minimize the joint error by reducing the gap in both feature and label differences, rather than focusing solely on feature differences. The label difference is crucial in cross-domain counting scenarios, leading performance decay for significant label domain shift. We demonstrate that aligning feature partitions based on partition attributes preserves task-relevant information within the label distribution of the target domain, promoting the generalization of the model.

# 4 Experiments and Results

## 4.1 Experiment Setting

We conduct the experiments on eight domain combinations of different counting scenarios, including crowd counting and cell counting, to examine the adaptability of BiAN. For the crowd-counting task, the combination include "Stadium"(SD)-"Street"(SR) and "Snow"(SN)-"Fog/Haze"(FH) within JHUCrowd++ (Sindagi et al., 2022), "Part A"(SHA)-"Part B"(SHB) within ShanghaiTech (Zhang et al., 2016), "Synthetic Fluorescence Microscopy"(VGG) (Xie et al., 2018b)-"Human subcutaneous adipose tissue"(ADI) dataset (Cohen et al., 2017), and "Dublin Cell Counting" (DCC) dataset (Marsden et al., 2018). The domain shift of crowd scenarios, including various weathers and densities, requires higher adaptability of the algorithm. For the cell counting task, the slight deviation of the cell amount of each image provides a comparative consistent density. However, various types of cells further challenge the performance of the model in the adaptability of scene presentation. The details of datasets and implementation are presented in Appendix A.6 and Appendix A.7. As to the evaluation metrics, we follow the previous works' setting. We employ only mean

Table 2: Counting MAE and MSE on crowd counting dataset ShanghaiTechA/B. The best are highlighted in bold. DA: Domain Adaptation for short.

| Methods | DA | SHB → SHA | | SHA → SHB | |
|---|---|---|---|---|---|
| | | MAE ↓ | MSE ↓ | MAE ↓ | MSE ↓ |
| CSRNet (Shi et al., 2019) | ✗ | 68.2 | 115.0 | 10.6 | 16.0 |
| KDM (Wan et al., 2022) | ✗ | 63.8 | 99.2 | 7.8 | 12.7 |
| UOT (Ma et al., 2021) | ✗ | 58.1 | 95.9 | 6.5 | 10.2 |
| STEERER (Han et al., 2023) | ✗ | 54.5 | 86.9 | 5.8 | 8.5 |
| CGNN (Zhang et al., 2024a) | ✗ | 61.1 | 97.8 | 7.7 | 13.0 |
| Cycle GAN (Zhu et al., 2017) | ✔ | 143.3 | 204.3 | 25.4 | 39.7 |
| SE CycleGAN (Wang et al., 2019b) | ✔ | 123.4 | 193.4 | 19.9 | 28.3 |
| BiTCC (Liu et al., 2020) | ✔ | 112.2 | 218.1 | 13.3 | 29.2 |
| LDG (Zhang et al., 2023) | ✔ | 118.5 | 190.1 | 14.2 | 25.2 |
| DGCC Du et al. (2023) | ✔ | 121.8 | 203.1 | 12.6 | 24.6 |
| SaKnD Xie et al. (2023a) | ✔ | 137.2 | 224.2 | 17.1 | 27.7 |
| CGNN-DA (Zhang et al., 2024a) | ✔ | 110.2 | 182.5 | 15.8 | 27.2 |
| BiAN (Ours) | ✔ | **42.3** | **53.0** | **5.7** | **7.2** |

absolute error (MAE) on cell counting as an evaluation metric, MAE and root mean squared error (MSE) on crowd-counting. Lower MAE and MSE indicate more precise counting results. This can be formulated as $MAE = \frac{1}{n}\sum_{i=1}^{n}|y_i - \hat{y}_i|$, $MSE = \sqrt{\frac{1}{n}\sum_{i=1}^{n}(y_i - \hat{y}_i)^2}$, which $y_i$ is the ground-truth count of the sample and $\hat{y}_i$ is the predication counts from model.

### 4.2 Performance Comparison and Analysis

This section presents the results of our experiments on the baseline and the latest state-of-the-art models, categorized into two distinct scenarios: crowd counting and cell counting. The crowd-counting scenario presents a high-density variation situation. By applying established counting methodologies to datasets within both domains, we set the groundwork for assessing BiAN's advancements.

Table 3: Counting MAE on cell counting dataset combinations. The best are highlighted in bold. DA: Domain Adaptation for short.

| Methods | DA | VGG → ADI | VGG → DCC |
|---|---|---|---|
| | | MAE↓ | MAE↓ |
| Counting Focus (Shi et al., 2019) | ✗ | – | 3.2 |
| CCF (Jiang & Yu, 2020) | ✗ | 14.5 | – |
| AECC (Wang et al., 2021) | ✗ | 14.1 | 3.0 |
| SAU-Net (Guo et al., 2022) | ✗ | 14.2 | 3.0 |
| Two-Path Net (Jiang & Yu, 2021) | ✗ | 10.6 | – |
| MSCA-UNet (Qian et al., 2023) | ✗ | 9.8 | – |
| DTLCC (Wang, 2023) | ✔ | – | 3.0 |
| IDN (Liu et al., 2024) | ✔ | 11.1 | – |
| BiAN (Ours) | ✔ | **9.2** | **2.7** |

The experimental results, presented in Table 2 and Table 1, demonstrate that BiAN not only surpasses the latest state-of-the-art DA/DG methods but also achieves precision comparable to fully supervised methods in some combinations. These findings indicate that BiAN effectively adapts to cross-scene crowd counting scenarios. The results shows that BiAN

423 424 425 426 427 428 429 430 431 432 433 434 435 436 437 438 439 440 441 442 443 444 445 446 447 448 449 450 451 452 453 454 455 456 457 458 459 460 461 462 463 464 465 466 467 468 469

significantly improves counting precision over the latest state-of-the-art methods. These findings indicate that BiAN effectively adapts to cross-scene crowd counting scenarios.

Overall, the compared models cover supervised methods and adaptation methods. The counting approach of models includes density estimation, point-to-point prediction, and point-to-density prediction. In both cases, BiAN performs better than SOTA methods on counting tasks, demonstrating the effectiveness of our method. We present additional experiment analysis in Appendices, including the experiments on the setting of synthetic-real crowd counting (Appendix A.8), and qualitative investigation between condition feature consistency and counting results (Appendix A.8.2), and visualization results (Appendix A.10).

### 4.3 Ablation Study

This section presents an ablation study to validate the effectiveness of our proposed method. We begin by removing all newly introduced mechanisms from the training process and implement all variants across both counting tasks. The unconditional variant applies domain alignment to the entire condition partitions without aligning conditions independently, failing to retain the target task-relevant feature distribution It presents adaptation via style transfer. The variant *w/o* CM employs conditional alignment but excludes the CM module. The experimental results are shown in Table 4. It can be observed that the unconditional alignment domain adaptation only has limited adaptability. In adapting DCC, the unconditional-only variant performs worse than the existing adaptations due to the significant difference in the visual character of the cell between the two domains. It indicates that the marginal difference between the two label spaces might be significant. According to the findings in (Zhao et al., 2019), the model is hard to find the optimal combination of parameters to minimize joint errors.

Table 4: Ablation study evaluated by MAE.

| $MAE \downarrow$ | Unconditional | BiAN *w/o* CM | BiAN |
|---|---|---|---|
| VGG → ADI | 14.8 | 10.1 (-4.7) | 9.2 (-5.6) |
| VGG → DCC | 3.6 | 3.4 (-0.2) | 2.7 (-0.9) |
| GCC → UCF | 35.0 | 32.7 (-2.3) | 22.7 (-12.3) |
| SHB → SHA | 58.9 | 46.0 (-12.9) | 42.3 (-16.6) |

In contrast, the samples in the crowd datasets share similar visual differences between partitions. Specifically, the scenes of the crowd are different. The difference between people and backgrounds is similar. In many instances, the background in crowd counting comprises other objects, leading to severe overlap situations compared to cell counting. In such cases, maintaining the margin distance between conditions is crucial. Incorporating the CM module noticeably enhances the adaptability of BiAN, demonstrating its ability to maintain condition-independent partitions. The ablation experiments provide strong empirical evidence supporting the effectiveness of our proposed model's design, offering a persuasive explanation for its superior performance.

## 5 Conclusion

This paper proposes Binary Alignment Network (BiAN) to mitigate the domain shift with preserving task-relevant information in UDA counting tasks. The proposed conditional alignment enables the network to maintain the inter-object contextual distribution when aligning feature distribution across domains. Augmented by our Condition-consistent Mechanism (CM), the segment map can be further refined, enhancing the robustness of BiAN. We also provide a theoretical demonstration with reasonable assumptions of how conditional alignment beneficial to our task. We implement comprehensive experiments to demonstrate the effectiveness of BiAN.

## REFERENCES

Shai Ben-David, John Blitzer, Koby Crammer, et al. A theory of learning from different domains. *Machine Learning*, 79(1-2):151–175, 2009. ISSN 0885-6125 1573-0565. doi: 10.1007/s10994-009-5152-4. 7

Konstantinos Bousmalis, George Trigeorgis, Nathan Silberman, Dilip Krishnan, and Dumitru Erhan. Domain separation networks. In *Proceedings of the 30th International Conference on Neural Information Processing Systems*, pp. 343–351. Curran Associates Inc., 2016. 1, 3

Ruichu Cai, Zijian Li, Pengfei Wei, Jie Qiao, Kun Zhang, and Zhifeng Hao. Learning disentangled semantic representation for domain adaptation. In *Proceedings of the Twenty-Eighth International Joint Conference on Artificial Intelligence*, pp. 2060–2066, 2019. doi: 10.24963/ijcai.2019/285. 3

Sungha Choi, Sanghun Jung, Huiwon Yun, Joanne T. Kim, Seungryong Kim, and Jaegul Choo. Robustnet: Improving domain generalization in urban-scene segmentation via instance selective whitening. In *2021 IEEE/CVF Conference on Computer Vision and Pattern Recognition (CVPR)*, pp. 11575–11585, 2021. doi: 10.1109/CVPR46437.2021.01141. 8

Joseph Paul Cohen, Geneviève Boucher, Craig A. Glastonbury, et al. Count-ception: Counting by fully convolutional redundant counting. In *2017 IEEE International Conference on Computer Vision Workshops (ICCVW)*, pp. 18–26, 2017. doi: 10.1109/ICCVW.2017.9. 8, 20

Nicolas Courty, Rémi Flamary, Amaury Habrard, and Alain Rakotomamonjy. Joint distribution optimal transportation for domain adaptation. In *Neural Information Processing Systems*, 2017. 3

Zhijie Deng, Yucen Luo, and Jun Zhu. Cluster alignment with a teacher for unsupervised domain adaptation. In *2019 IEEE/CVF International Conference on Computer Vision (ICCV)*, pp. 9943–9952, 2019. doi: 10.1109/iccv.2019.01004. 3

Zhipeng Du, Jiankang Deng, and Miaojing Shi. Domain-general crowd counting in unseen scenarios. In *Proceedings of the AAAI Conference on Artificial Intelligence*, volume 37, pp. 561–570. Association for the Advancement of Artificial Intelligence (AAAI), 2023. ISBN 2374-3468. doi: 10.1609/aaai.v37i1.25131. 8, 9

Cian Eastwood, Ian Mason, Chris Williams, and Bernhard Scholkopf. Source-free adaptation to measurement shift via bottom-up feature restoration. In *International Conference on Learning Representations*, 2022. 3

Yaroslav Ganin and Victor Lempitsky. Unsupervised domain adaptation by backpropagation. In *Proceedings of the 32nd International Conference on Machine Learning (ICML)*, volume 37, pp. 1180–1189, Lille, France, 07-09 Jul 2015. PMLR. 3, 5

Junyu Gao, Yuan Yuan, and Qi Wang. Feature-aware adaptation and density alignment for crowd counting in video surveillance. *IEEE Transactions on Cybernetics*, 51(10):4822–4833, 2021. ISSN 2168-2267. doi: 10.1109/tcyb.2020.3034316. 3

Yue Guo, Oleh Krupa, Jason Stein, et al. Sau-net: A unified network for cell counting in 2d and 3d microscopy images. *IEEE/ACM Transactions on Computational Biology and Bioinformatics*, 19(4):1920–1932, 2022. ISSN 1545-5963. doi: 10.1109/tcbb.2021.3089608. 3, 5, 9

Tao Han, Lei Bai, Lingbo Liu, and Wanli Ouyang. Steerer: Resolving scale variations for counting and localization via selective inheritance learning. In *2023 IEEE/CVF International Conference on Computer Vision (ICCV)*. IEEE, 2023. doi: 10.1109/iccv51070.2023.01997. 2, 3, 9, 21

Shenghua He, Kyaw Thu Minn, Lilianna Solnica-Krezel, Mark A. Anastasio, and Hua Li. Deeply-supervised density regression for automatic cell counting in microscopy images. *Med Image Anal*, 68:101892, 2021. ISSN 1361-8423 (Electronic) 1361-8415 (Print) 1361-8415 (Linking). doi: 10.1016/j.media.2020.101892. 1

Haroon Idrees, Muhmmad Tayyab, Kishan Athrey, et al. Composition loss for counting, density map estimation and localization in dense crowds. In *Computer Vision - ECCV 2018*, pp. 544–559, Cham, 2018. Springer International Publishing. ISBN 978-3-030-01216-8. 19

Junguang Jiang, Baixu Chen, Jianmin Wang, and Mingsheng Long. Decoupled adaptation for cross-domain object detection. In *The Tenth International Conference on Learning Representations, ICLR 2022, Virtual Event, April 25-29, 2022*. OpenReview.net, 2022. 3, 17

Ni Jiang and Feihong Yu. A cell counting framework based on random forest and density map. *Applied Sciences*, 10(23):8346, 2020. ISSN 2076-3417. doi: 10.3390/app10238346. 9

Ni Jiang and Feihong Yu. A two-path network for cell counting. *IEEE Access*, 9:70806–70815, 2021. ISSN 2169-3536. doi: 10.1109/access.2021.3078481. 9

Xiaoheng Jiang, Li Zhang, Tianzhu Zhang, et al. Density-aware multi-task learning for crowd counting. *IEEE Transactions on Multimedia*, 23:443–453, 2021. doi: 10.1109/TMM.2020.2980945. 3

Matthieu Kirchmeyer, Alain Rakotomamonjy, Emmanuel de Bezenac, and patrick gallinari. Mapping conditional distributions for domain adaptation under generalized target shift. In *International Conference on Learning Representations*, 2022. 3

Lingjing Kong, Shaoan Xie, Weiran Yao, Yujia Zheng, Guangyi Chen, Petar Stojanov, Victor Akinwande, and Kun Zhang. Partial disentanglement for domain adaptation. In Chaudhuri Kamalika, Jegelka Stefanie, Song Le, Szepesvari Csaba, Niu Gang, and Sabato Sivan (eds.), *Proceedings of the 39th International Conference on Machine Learning*, volume 162, pp. 11455–11472. PMLR, 2022. URL `https://proceedings.mlr.press/v162/kong22a.html`. 1, 3, 4

Ruihuang Li, Xu Jia, Jianzhong He, Shuaijun Chen, and Qinghua Hu. T-svdnet: Exploring high-order prototypical correlations for multi-source domain adaptation. In *2021 IEEE/CVF International Conference on Computer Vision (ICCV)*, pp. 9971–9980, 2021. doi: 10.1109/iccv48922.2021.00984. 4

Wang Li, Li Yongbo, and Xue Xiangyang. Coda: Counting objects via scale-aware adversarial density adaption. In *2019 IEEE International Conference on Multimedia and Expo (ICME)*, pp. 193–198. IEEE, 2019. doi: 10.1109/icme.2019.00041. 2, 3

Hui Lin, Zhiheng Ma, Rongrong Ji, Yaowei Wang, and Xiaopeng Hong. Boosting crowd counting via multifaceted attention. In *2022 IEEE/CVF Conference on Computer Vision and Pattern Recognition (CVPR)*, pp. 19596–19605, 2022. doi: 10.1109/CVPR52688.2022.01901. 8

Lei Liu, Jie Jiang, Wenjing Jia, et al. Denet: A universal network for counting crowd with varying densities and scales. *IEEE Transactions on Multimedia*, 23:1060–1068, 2021. doi: 10.1109/TMM.2020.2992979. 3

Rui Liu, Yudi Zhu, Cong Wu, Hao Guo, Wei Dai, Tianyi Wu, Min Wang, Wen Jung Li, and Jun Liu. Interactive dual network with adaptive density map for automatic cell counting. *IEEE Transactions on Automation Science and Engineering*, pp. 1–13, 2024. ISSN 1545-5955 1558-3783. doi: 10.1109/tase.2023.3329973. 9

Yahao Liu, Jinhong Deng, Jiale Tao, Tong Chu, Lixin Duan, and Wen Li. Undoing the damage of label shift for cross-domain semantic segmentation. In *2022 IEEE/CVF Conference on Computer Vision and Pattern Recognition (CVPR)*, pp. 7032–7042, 2022. doi: 10.1109/cvpr52688.2022.00691. 3

Yuting Liu, Zheng Wang, Miaojing Shi, et al. Towards unsupervised crowd counting via regression-detection bi-knowledge transfer. In *Proceedings of the 28th ACM International Conference on Multimedia (MM)*, MM '20, pp. 129–137, New York, NY, USA, 2020. ACM. ISBN 9781450379885. doi: 10.1145/3394171.3413825. 9

Mingsheng Long, Zhangjie Cao, Jianmin Wang, and Michael I. Jordan. Conditional adversarial domain adaptation. In *Proceedings of the 32nd International Conference on Neural Information Processing Systems*, pp. 1647–1657. Curran Associates Inc., 2018. 4

John Lonsdale, Jeffrey Thomas, Mike Salvatore, et al. The genotype-tissue expression (gtex) project. *Nature Genetics*, 45(6):580–585, Jun 2013. ISSN 1546-1718. doi: 10.1038/ng.2653. 20

Chen Change Loy, Shaogang Gong, and Tao Xiang. From semi-supervised to transfer counting of crowds. In *2013 IEEE International Conference on Computer Vision (ICCV)*, pp. 2256–2263. IEEE, 2013. doi: 10.1109/ICCV.2013.270. 3

Zhiheng Ma, Xing Wei, Xiaopeng Hong, and Yihong Gong. Bayesian loss for crowd count estimation with point supervision. In *2019 IEEE/CVF International Conference on Computer Vision (ICCV)*, pp. 6141–6150, 2019. doi: 10.1109/iccv.2019.00624. 8

Zhiheng Ma, Xing Wei, Xiaopeng Hong, Hui Lin, Yunfeng Qiu, and Yihong Gong. Learning to count via unbalanced optimal transport. In *Proceedings of the AAAI Conference on Artificial Intelligence*, volume 35, pp. 2319–2327, 2021. ISBN 2374-3468 2159-5399. doi: 10.1609/aaai.v35i3.16332. 9, 21

Haitao Mao, Lun Du, Yujia Zheng, Qiang Fu, Zelin Li, Xu Chen, Shi Han, and Dongmei Zhang. Source free graph unsupervised domain adaptation. In *Proceedings of the 17th ACM International Conference on Web Search and Data Mining*, pp. 520–528. Association for Computing Machinery, 2024. doi: 10.1145/3616855.3635802. URL https://doi.org/10.1145/3616855.3635802. 3

Mark Marsden, Kevin McGuinness, Suzanne Little, et al. People, penguins and petri dishes: Adapting object counting models to new visual domains and object types without forgetting. In *2018 IEEE/CVF Conference on Computer Vision and Pattern Recognition (CVPR)*, pp. 8070–8079, 2018. doi: 10.1109/CVPR.2018.00842. 8, 20

Xingang Pan, Ping Luo, Jianping Shi, and Xiaoou Tang. Two at once: Enhancing learning and generalization capacities via ibn-net. In *Computer Vision – ECCV 2018*, Computer Vision – ECCV 2018, pp. 484–500. Springer International Publishing, 2018. ISBN 978-3-030-01225-0. doi: 10.1007/978-3-030-01225-0_29. 8

Xingang Pan, Xiaohang Zhan, Jianping Shi, Xiaoou Tang, and Ping Luo. Switchable whitening for deep representation learning. In *2019 IEEE/CVF International Conference on Computer Vision (ICCV)*, pp. 1863–1871, 2019. doi: 10.1109/ICCV.2019.00195. 8

Geon Yeong Park and Sang Wan Lee. Information-theoretic regularization for multi-source domain adaptation. In *2021 IEEE/CVF International Conference on Computer Vision (ICCV)*, pp. 9194–9203, 2021. doi: 10.1109/iccv48922.2021.00908. 4

Xingchao Peng, Qinxun Bai, Xide Xia, Zijun Huang, Kate Saenko, and Bo Wang. Moment matching for multi-source domain adaptation. In *2019 IEEE/CVF International Conference on Computer Vision (ICCV)*, pp. 1406–1415, 2019. doi: 10.1109/iccv.2019.00149. 4

Zhuoxuan Peng and S. H. Gary Chan. Single domain generalization for crowd counting. In *2024 IEEE/CVF Conference on Computer Vision and Pattern Recognition (CVPR)*, pp. 28025–28034, 2024. doi: 10.1109/cvpr52733.2024.02647. 8

Like Qian, Wei Qian, Dingcheng Tian, Yaqi Zhu, Heng Zhao, and Yudong Yao. Msca-unet: Multi-scale convolutional attention unet for automatic cell counting using density regression. *IEEE Access*, 11:85990–86001, 2023. ISSN 2169-3536. doi: 10.1109/access.2023.3304993. 9

Becca Roelofs, David Berthelot, Kihyuk Sohn, Nicholas Carlini, and Alex Kurakin. Adamatch: A unified approach to semi-supervised learning and domain adaptation. In *International Conference on Learning Representations*, 2022. 3

Zenglin Shi, Pascal Mettes, and Cees Snoek. Counting with focus for free. In *2019 IEEE/CVF International Conference on Computer Vision (ICCV)*, pp. 4199–4208. IEEE, 2019. doi: 10.1109/iccv.2019.00430. 9

Rui Shu, Hung Bui, Hirokazu Narui, and Stefano Ermon. A dirt-t approach to unsupervised domain adaptation. In *International Conference on Learning Representations*, 2018. 4

V. A. Sindagi, R. Yasarla, and V. M. Patel. Jhu-crowd++: Large-scale crowd counting dataset and a benchmark method. *IEEE Trans Pattern Anal Mach Intell*, 44(5):2594–2609, 2022. ISSN 1939-3539 (Electronic) 0098-5589 (Linking). doi: 10.1109/TPAMI.2020.3035969. URL https://www.ncbi.nlm.nih.gov/pubmed/33147141. Sindagi, Vishwanath A Yasarla, Rajeev Patel, Vishal M eng Research Support, U.S. Gov't, Non-P.H.S. 2020/11/05 IEEE Trans Pattern Anal Mach Intell. 2022 May;44(5):2594-2609. doi: 10.1109/TPAMI.2020.3035969. Epub 2022 Apr 1. 8, 19

Peeyush Singhal, Rahee Walambe, Sheela Ramanna, et al. Domain adaptation: Challenges, methods, datasets, and applications. *IEEE Access*, 11:6973–7020, 2023. ISSN 2169-3536. doi: 10.1109/access.2023.3237025. 1

Petar Stojanov, Zijian Li, Mingming Gong, Ruichu Cai, Jaime G. Carbonell, and Kun Zhang. Domain adaptation with invariant representation learning: what transformations to learn? In *Proceedings of the 35th International Conference on Neural Information Processing Systems*, pp. Article 1899. Curran Associates Inc., 2024. 3

Shangyuan Tong, Timur Garipov, Yang Zhang, Shiyu Chang, and Tommi S. Jaakkola. Adversarial support alignment. In *International Conference on Learning Representations*, 2022. 3

Eric Tzeng, Judy Hoffman, Kate Saenko, and Trevor Darrell. Adversarial discriminative domain adaptation. In *2017 IEEE Conference on Computer Vision and Pattern Recognition (CVPR)*, pp. 2962–2971, 2017. doi: 10.1109/cvpr.2017.316. 3

Jia Wan, Qingzhong Wang, and Antoni B. Chan. Kernel-based density map generation for dense object counting. *IEEE Transactions on Pattern Analysis and Machine Intelligence*, 44(3):1357–1370, 2022. ISSN 0162-8828. doi: 10.1109/tpami.2020.3022878. 3, 9, 21

Hang Wang, Minghao Xu, Bingbing Ni, and Wenjun Zhang. Learning to combine: Knowledge aggregation for multi-source domain adaptation. In *Computer Vision – ECCV 2020*, Computer Vision – ECCV 2020, pp. 727–744. Springer International Publishing, 2020. ISBN 978-3-030-58598-3. 4

Jindong Wang, Yiqiang Chen, Han Yu, Meiyu Huang, and Qiang Yang. Easy transfer learning by exploiting intra-domain structures. In *2019 IEEE International Conference on Multimedia and Expo (ICME)*, pp. 1210–1215, 2019a. doi: 10.1109/icme.2019.00211. 3

Qi Wang, Junyu Gao, Wei Lin, et al. Learning from synthetic data for crowd counting in the wild. In *2019 IEEE/CVF Conference on Computer Vision and Pattern Recognition (CVPR)*, pp. 8190–8199, 2019b. doi: 10.1109/CVPR.2019.00839. 1, 3, 9, 19, 21

Shanshan Wang, Cheng Li, Rongpin Wang, et al. Annotation-efficient deep learning for automatic medical image segmentation. *Nature Communications*, 12(1), 2021. ISSN 2041-1723. doi: 10.1038/s41467-021-26216-9. 9

Zuhui Wang. Cross-domain microscopy cell counting by disentangled transfer learning. In *Trustworthy Machine Learning for Healthcare*, pp. 93–105. Springer Nature Switzerland, 2023. ISBN 0302-9743. doi: 10.1007/978-3-031-39539-0_9. 9

Zongze Wu, Yotam Nitzan, Eli Shechtman, and Dani Lischinski. Stylealign: Analysis and applications of aligned stylegan models. In *International Conference on Learning Representations*, 2022. 3

Haiyang Xie, Zhengwei Yang, Huilin Zhu, and Zheng Wang. Striking a balance: Unsupervised cross-domain crowd counting via knowledge diffusion. In *Proceedings of the 31st ACM International Conference on Multimedia (MM)*, pp. 6520–6529, 2023a. doi: 10.1145/3581783.3611797. 3, 9

Shaoan Xie, Zibin Zheng, Liang Chen, and Chuan Chen. Learning semantic representations for unsupervised domain adaptation. In Dy Jennifer and Krause Andreas (eds.), *Proceedings of the 35th International Conference on Machine Learning*, volume 80, pp. 5423–5432. PMLR, 2018a. URL `https://proceedings.mlr.press/v80/xie18c.html`. 4

Shaoan Xie, Lingjing Kong, Mingming Gong, and Kun Zhang. Multi-domain image generation and translation with identifiability guarantees. In *The Eleventh International Conference on Learning Representations*, 2023b. URL `https://openreview.net/forum?id=U2g8OGONA_V`. 1

Weidi Xie, J. Alison Noble, and Andrew Zisserman. Microscopy cell counting and detection with fully convolutional regression networks. *Computer Methods in Biomechanics and Biomedical Engineering: Imaging & Visualization*, 6(3):283–292, 2018b. doi: 10.1080/21681163.2016.1149104. 8, 20

Ruijia Xu, Ziliang Chen, Wangmeng Zuo, Junjie Yan, and Liang Lin. Deep cocktail network: Multi-source unsupervised domain adaptation with category shift. In *2018 IEEE/CVF Conference on Computer Vision and Pattern Recognition*, pp. 3964–3973, 2018. doi: 10.1109/cvpr.2018.00417. 4

Ruijia Xu, Guanbin Li, Jihan Yang, and Liang Lin. Larger norm more transferable: An adaptive feature norm approach for unsupervised domain adaptation. In *2019 IEEE/CVF International Conference on Computer Vision (ICCV)*, pp. 1426–1435, 2019. doi: 10.1109/iccv.2019.00151. 3

Tongkun Xu, Weihua Chen, Pichao WANG, Fan Wang, Hao Li, and Rong Jin. Cdtrans: Cross-domain transformer for unsupervised domain adaptation. In *International Conference on Learning Representations*, 2022. 3

Siya Yao, Qi Kang, Mengchu Zhou, Muhyaddin J. Rawa, and Aiiad Albeshri. Discriminative manifold distribution alignment for domain adaptation. *IEEE Transactions on Systems, Man, and Cybernetics: Systems*, 53(2):1183–1197, 2023. ISSN 2168-2216. doi: 10.1109/tsmc.2022.3195239. 17

Anran Zhang, Yandan Yang, Jun Xu, et al. Latent domain generation for unsupervised domain adaptation object counting. *IEEE Transactions on Multimedia*, 25:1773–1783, 2023. ISSN 1520-9210. doi: 10.1109/tmm.2022.3162710. 3, 9

Chengyang Zhang, Yong Zhang, Bo Li, Xinglin Piao, and Baocai Yin. Crowdgraph: Weakly supervised crowd counting via pure graph neural network. *ACM Transactions on Multimedia Computing, Communications, and Applications*, 20(5):1–23, 2024a. ISSN 1551-6857. doi: 10.1145/3638774. 3, 9

Jing Zhang, Wanqing Li, and Philip Ogunbona. Joint geometrical and statistical alignment for visual domain adaptation. In *2017 IEEE Conference on Computer Vision and Pattern Recognition (CVPR)*, pp. 5150–5158, 2017. doi: 10.1109/cvpr.2017.547. 3

Kun Zhang, Mingming Gong, Petar Stojanov, Biwei Huang, Qingsong Liu, and Clark Glymour. Domain adaptation as a problem of inference on graphical models. In *Proceedings of the 34th International Conference on Neural Information Processing Systems*, pp. Article 417. Curran Associates Inc., 2020. 3

Libo Zhang, Wenzhang Zhou, Heng Fan, Tiejian Luo, and Haibin Ling. Robust domain adaptive object detection with unified multi-granularity alignment. *IEEE Trans Pattern Anal Mach Intell*, 46(12):9161–9178, 2024b. ISSN 1939-3539 (Electronic) 0098-5589 (Linking). doi: 10.1109/TPAMI.2024.3416098. 3, 17

Yingying Zhang, Desen Zhou, Siqin Chen, et al. Single-image crowd counting via multi-column convolutional neural network. In *2016 IEEE Conference on Computer Vision and Pattern Recognition (CVPR)*, pp. 589–597, 2016. doi: 10.1109/CVPR.2016.70. 8, 19

Han Zhao, Remi Tachet Des Combes, Kun Zhang, et al. On learning invariant representations for domain adaptation. In *Proceedings of the 36th International Conference on Machine Learning (ICML)*, volume 97, pp. 7523–7532. PMLR, 09-15 Jun 2019. 4, 7, 10, 26

Huilin Zhu, Jingling Yuan, Xian Zhong, Zhengwei Yang, Zheng Wang, and Shengfeng He. Daot: Domain-agnostically aligned optimal transport for domain-adaptive crowd counting. In *Proceedings of the 31st ACM International Conference on Multimedia*, pp. 4319–4329. Association for Computing Machinery, 2023. ISBN 9798400701085. doi: 10.1145/3581783.3611793. 8

Jun-Yan Zhu, Taesung Park, Phillip Isola, and Alexei A. Efros. Unpaired image-to-image translation using cycle-consistent adversarial networks. In *2017 IEEE International Conference on Computer Vision (ICCV)*, pp. 2242–2251, 2017. doi: 10.1109/iccv.2017.244. 9, 21

Peihao Zhu, Rameen Abdal, John Femiani, and Peter Wonka. Mind the gap: Domain gap control for single shot domain adaptation for generative adversarial networks. In *International Conference on Learning Representations*, 2022. 3

# A APPENDIX

## A.1 MORE RELATED WORK

In Unsupervised Domain Adaptation (UDA), there are common to adopt the component-wise alignment to align the feature distribution across domains. The most common method is to align the marginal distribution of the feature space (Jiang et al., 2022; Zhang et al., 2024b; Yao et al., 2023). MGA (Zhang et al., 2024b) designs category-level discriminator to align the distributions on the category-level. D-adapt (Jiang et al., 2022) deploys the bounding box alignment for mitigating the domain shift on object-level. Our method is actually different from these methods. Their goal is only to align the distribution of object-relevant features under the assumption that unconditional alignment can reduce the joint decision error all the time. It also assumes that the unconditional alignment will not violate the inter-object contextual distribution. However, in the object counting task, these assumptions are not maintained. One of the crucial assumptions in our method is that there are no overlap between the condition partitions during the alignment. And the designed CM module is to maintain the condition-independent partitions. The proposed BiAN is designed to align the feature distribution across domains while preserving the inter-object information by maintaining the condition-independent partitions. The proposed method is more suitable for the object counting task.

## A.2 TRAINING PROCESS

Here we provide the detailed training procedure of BiAN. The training process is shown in Algorithm A.2. The training process is similar to the standard training process of UDA. The difference is that we introduce the conditional alignment and the CM module to the training process. The images $(x_s, x_t)$ from the source and target domain are fed into the model $h = g_{s/t} \circ f$. The model firstly predicts the counting results $\hat{y}_s$ and $\hat{y}_t$. Then model segments the images into foreground and background using the predicted results, obtaining $(x_s^f, x_s^b)$ and $(x_t^f, x_t^b)$. The model then predicts the conditional results $(\hat{y}_s^f, \hat{y}_s^b)$ and $(\hat{y}_t^f, \hat{y}_t^b)$ for the foreground and background. The conditional domain loss $\mathcal{L}_{\text{d}}$ is calculated between the conditional results. The pixel loss $\mathcal{L}_p$ is calculated between the predicted results and the ground truth. The source loss $\mathcal{L}_{\text{source}}$ and the target loss $\mathcal{L}_{\text{target}}$ are calculated. The CM loss $\mathcal{L}_{\text{CM}}$ is calculated between the conditional results and the predicted results. The sum up loss $\mathcal{L}$ is calculated. The gradient of the loss is calculated and the model is updated.

## A.3 PROOF OF LEMMA 2

*Proof.*

$$d_{\mathcal{C}}\left(\mathcal{Y}, \mathcal{Y}'\right) = \sum_{i \in [1,k]} d_{JS}\left(\mathcal{Y}_i, \mathcal{Y}_i'\right),$$

According to the definition, the samples within the condition subsets share the same label. So that, according to the previous definition of $d_{JS}\left(D, D'\right)$, we have for every $i \in [1, k]$:

$$d_{\mathcal{C}}\left(\mathcal{Y}, \mathcal{Y}'\right) = 0,$$

□

## A.4 PROOF OF LEMMA 3

*Proof.* According to Definition 3, we have

$$D_i^c \cap D_j'^c = \varnothing, i \neq j.$$

**Algorithm 1** Training Procedure of BiAN

**Require:** Source dataset $\mathcal{D}_s$, Target dataset $\mathcal{D}_t$, Model parameters $\theta$, Learning rate $\eta$, Epochs $E$
**Ensure:** Trained model parameters $\theta$

```
for epoch = 1 to E do
    Shuffle dataset D_s, D_t
    for each batch B = (x_s, x_t) do
        Compute predictions ŷ_s, ŷ_t using model with parameters θ
        Get (x_s^f, x_s^b), (x_t^f, x_t^b) segmenting x_s, x_t with ŷ_s, ŷ_t
        Compute conditional predictions (ŷ_s^f, ŷ_s^b),(ŷ_t^f, ŷ_t^b) using model with parameters θ
        Compute conditional domain loss L_d between (ĉ_s^f, ĉ_t^f) and (ĉ_s^b, ĉ_t^b)
        Calculate pixel loss L_p between ŷ_s and ground truth y_s
        Calculate L_source and L_target
        Calculate CM loss L_CM between (ŷ_t^f, ŷ_t^b) and ŷ_t
        Calculate sum up loss L = L_source + L_target + λL_CM
        Reverse the gradient of L_d then compute gradient ∇_θ L
        Update parameters: θ ← θ − η · ∇_θ L
    end for
    if early stopping condition is met then
        break
    end if
end for
return θ
```

This implies that the subsets $D_i^c$ and $D_j'^c$ are disjoint whenever $i \neq j$. Since $D'$ can be expressed as the union of all such $D_j'^c$, for any $x \in D'$, it specifically lies in one of these subsets $D_i'^c$ if $x$ also belongs to $D_i^c$. Therefore, we have:

$$x \in D_i^c \cap D' \implies x \in D_i^c \cap D_i'^c.$$

Since $D_i^c \cap D' = D_i^c \cap D_i'^c$, the Jensen-Shannon divergence calculation between $D_i^c$ and $D'$ simplifies to:

$$d_{JS}(D_i^c, D') = d_{JS}(D_i^c, D_i'^c).$$

This holds because the overlap between $D_i^c$ and $D'$ is exactly $D_i^c$ and $D_i'^c$, thus limiting the scope of the divergence calculation to these intersecting subsets. □

### A.5 Proof of Conditional Alignment

*Proof.* The situation of the large marginal difference on label space can be represented as follows. Given condition set $\mathcal{Y} = \{c_1, c_2, c_3, \ldots, c_k\}$, for any $i \in [1, k]$, we have:

$$Y_i^c \cap Y' = Y_j'^c, i \neq j.$$

Without loss of generality, we suppose $j = i + 1$, so that we have:

$$d_{JS}\left(Y, Y'\right) = \sum_{i=1}^{k} d_{JS}\left(Y_i^c, Y_j'^c\right).$$

Specially, we set $Y_{k+1}'^c = Y_1'^c$.

We have conditional aligned domains $D$ and $D'$, which can be represented as:

$$d_{\mathcal{C}}\left(D, D'\right) = 0.$$

Therefore, for any $i \in [1, k]$:

$$d_{JS}\left(D_i^c, D_i'^c\right) = 0.$$

We have conditional aligned $\mathcal{Y}$ and $\mathcal{Y}'$, so it can instantly have:

$$d_{JS}\left(D_i'^c, Y_i'^c\right) = 0.$$

Combineing the equations above, we have:

$$d_{JS}\left(D_i^c, Y_i'^c\right) = 0.$$

According to Lemma 2, we have:

$$d_{JS}\left(Y_i^c, Y_j'^c\right) = d_{JS}\left(D_i^c, Y_j^c\right) = d_{JS}\left(D_i^c, D_j^c\right) = d_{JS}\left(D_i^c, D_j'^c\right).$$

It is possible to find an order of sorting the $D_i^c$ and $D_i'^c$, so that the JS-convergence between $D$ and $D'$ can be:

$$d_{JS}\left(D, D'\right) = \sum_{i=1}^{k} d_{JS}\left(D_i^c, D_j'^c\right).$$

Specifically, we set $D_{k+1}'^c = D_1'^c$. To this end, combining the equations above, we have:

$$d_{JS}\left(D, D'\right) = d_{JS}\left(Y, Y'\right).$$

□

### A.6 Dataset Details

In this section, we will provide details about the dataset we implemented in our experiments, including cell counting datasets and crowd counting datasets. Example visualization is shown as Figure 3.

For the crowd-counting task, the datasets include GTA5 Crowd Counting (GCC) (Wang et al., 2019b), UCF-QNRF (UCF) (Idrees et al., 2018), ShanghaiTech (SHA & SHB) (Zhang et al., 2016), and JHU-Crowd++Sindagi et al. (2022). The details of the crowd dataset are shown as follows:

- GCC (Wang et al., 2019b) is generated from multiple crowd scenes in Grand Theft Auto V, a video game, with 15,210 samples. The image size is 1920×1080 pixels. The synthetic environment contains multiple times of the day, seven types of weather, and diverse scenes (e.g. beach, street, and other common public scenes.). It provides various simulations of real-world scenes. The average of crowded count for each image is 500, with the highest count of 4000 and lowest count of zero.
- UCF (Idrees et al., 2018) is a large-scale dataset that contains 1535 high solution images with considerable crowd variation. The images are obtained from the Web by multiple platforms. So, the resolutions are highly dynamic. The average density of images is 1000 counts but with a standard deviation 7605.14.
- The ShanghaiTech (Zhang et al., 2016) dataset consists of parts A and B, containing 482 and 716 samples, respectively. Part A (SHA) is obtained from the Web with dynamic resolutions. The mean of counts per image is 541, with a standard deviation of 504. Part B (SHB) is retrieved from the security monitoring cameras on busy streets with fixed resolutions. The mean of counts per image is 122, with a standard deviation 93.
- The JHUCrowd++ (Sindagi et al., 2022) dataset consists of 4,372 images with detailed annotations, totaling approximately 1.51 million instances. The images are collected from diverse sources, including the web and surveillance cameras, featuring varying resolutions and perspectives. The dataset captures a wide range of crowd densities, from sparse to extremely dense scenes. The mean count per image is approximately 346, with a standard deviation of 1,094, indicating significant variability in crowd counts across the dataset.

The environments of the crowd datasets, including various weathers and scenes, are among the most challenging issues to handle in crowd counting. It requires algorithms with higher adaptability to handle it. Overall, the selection of datasets covers a sufficient variety of environments and scenes. In the following experiments, we examine the transferability of the BiAN by evaluating its performance in transferring features between the domains from the datasets shown above.

For the cell counting task, the datasets include three public benchmarks: synthetic fluorescence microscopy (VGG) dataset (Xie et al., 2018b), human subcutaneous adipose tissue (ADI) dataset (Cohen et al., 2017), and Dublin Cell Counting (DCC) dataset. The details of the cell dataset are shown as follows:

- VGG (Xie et al., 2018b) is a synthetic microscopy cell image dataset with 200 samples. It simulates bacterial cells from fluorescence-light microscopy at various focal distances. The size of microscopy images is maintained as 256×256 pixels. The cell amount of VGG for each image is 174±64.
- DCC (Marsden et al., 2018) dataset is built with 177 samples from various categories of cells from real cases, including embryonic mice stem cells, human lung adenocarcinoma, and monocytes. The image size ranges from 306×322 pixels to 798×788 pixels, due to obtained via dynamic zoom scope. Moreover, the cell amount for each image is 34±21, intended to increase the variation of the dataset.
- ADI (Cohen et al., 2017) is constructed from Genotype Tissue Expression Consortium (Lonsdale et al., 2013) with densely packed adipocyte cells from real cases. The dataset is built from 200 images. The image size is 150×150 pixels. The cell amount for each image is 165±44.

The slight deviation of the cell amount of each image provides a relative consistency in cell density. Various types of cells further challenge the performance of the model in the adaptability of scene presentation.

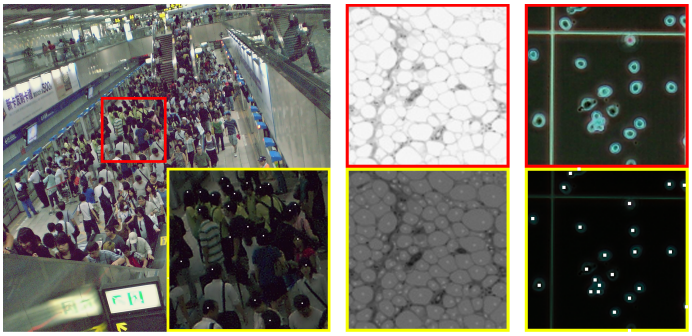

(a) (b) (c)

Figure 3: Object counting scenarios: (a) public security monitoring; (b) medical pathological analysis; (c) biological experiment.

### A.7 Experiment Implementation Details

We choose the Adam optimizer with decoupled weight decay. The learning rate for the optimizer is set to 1e-6, and the weight decay rate is 1e-4. For the learning rate, we use a step learning rate scheduler with a 10-epoch step to lower the learning rate by 0.1 for every step. To handle the limitation of GPU memory, we resize cell images to 128 × 128 pixels and crowd images to 96 × 96 pixels. Notably adopting the annotated counts before resizing the images to maintain the ground truth unaffected by squeezing. The coefficient $\alpha$ of CM loss is set to 100. Moreover, we apply the training scalar on the annotations to enhance the numeric difference. The scalar for VGG and ADI is 100. For DCC and all applied crowd datasets, it is set as 500,

respectively. BiAN is fully implemented in PyTorch, running on a single NVIDIA RTX 3090 with a single Intel® Core™ i7-10700 CPU @ 2.90GHz.

## A.8 Additional Experiment Analysis

### A.8.1 Source on Synthetic Crowd Dataset

Migrating from the source synthetic dataset to a real-world dataset is a practical approach to handling insufficient data annotation issues. To validate BiAN performance on such condition, we conduct the experiments with the setting of GCC (*source*) and UCF (*target*). Specifically, we have to resize the input to a smaller size (128×128 px) due to memory limitation. We have taken reasonable measures to preserve the information. The results still show that BiAn outperforms SOTA methods. But due to no guarantee on lost information, the experiment results only can be quantitatively referred.

Table 5: Counting MAE and MSE on crowd counting task from synthetic source. The best are highlighted in bold. DA: Domain Adaptation for short.

| Methods | DA | GCC → UCF | |
|---|---|---|---|
| | | MAE ↓ | MSE ↓ |
| KDMG (Wan et al., 2022) | ✗ | 99.5 | 173.0 |
| UOT (Ma et al., 2021) | ✗ | 83.3 | 142.3 |
| STEERER (Han et al., 2023) | ✗ | 74.3 | 128.3 |
| Cycle GAN (Zhu et al., 2017) | ✔ | 257.3 | 400.6 |
| SE CycleGAN (Wang et al., 2019b) | ✔ | 230.4 | 384.5 |
| BiAN (Ours) | ✔ | **22.7** | 28.4 |

### A.8.2 Relevance Analysis between Consistency and Counting Results

In this section, we further demonstrate the proposed Condition-Consistency Mechanism (CM), which benefits from reliable counting when there is a lack of precise annotation during the adaptation process. We plot the curves presenting the tendency of MAE on the validation set and uncertainty during the training period. Specifically, the uncertainty index is calculated by the normalized CM loss $NORM(\mathcal{L}_{CM})$, indicating how inconsistent the features of assembling conditions and entire ones are. It can be observed that the counting performance, which is inversely proportional to the MAE value, is promoted when the uncertainty index decays. Combined with the results in experiment results in Section 4.3, it can validate that the assumption on disjoint condition subsets is necessary in BiAN and conditional alignment framework.

## A.9 Model Architecture of BiAN

In this section, we present the architectural details of our proposed BiAN. As shown in Figure 2, the architecture can be divided into domain-specific feature extractors ($g_{S/T}$), density map regression layers ($f$), domain discriminator ($f_d$), condition-consistent layers ($f_c$). The total parameters amount of BiAN is 70,755,271 with an estimated model size of 2783.41 MB.

The domain-specific feature extractors ($g_{s/t}$), detailed in Appendix A.9, are responsible for capturing relevant features from the input data in both source and target domains. Specifically, the input is resized as 256×256 px. And the network arguments are independent among $g_s$ and $g_t$, but same architecture for similar feature retrieval.

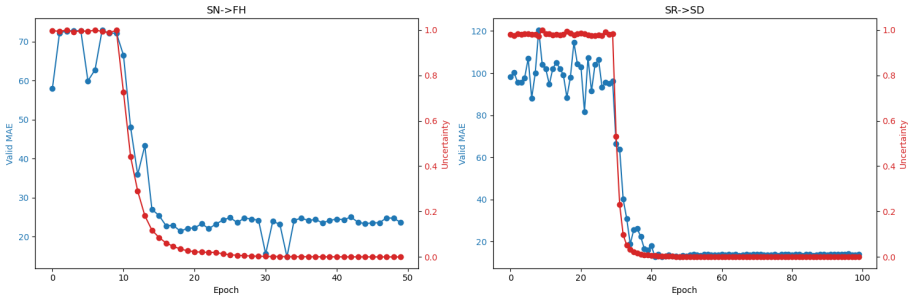


Figure 4: The tendency of validation counting MAE and the consistency on two domain combinations.

Table 6: Architecture of feature extractor in BiAN.

| Layer (Type: Depth-Idx) | Output Shape | Parameters (#) |
|---|---|---|
| Conv2d: 3-1 | [32, 256, 256] | 384 |
| Conv2d: 3-2 | [32, 256, 256] | 9,312 |
| MaxPool2d: 3-3 | [32, 128, 128] | – |
| Conv2d: 3-4 | [64, 128, 128] | 18,624 |
| Conv2d: 3-5 | [64, 128, 128] | 37,056 |
| MaxPool2d: 3-6 | [64, 64, 64] | – |
| Conv2d: 3-7 | [128, 64, 64] | 74,112 |
| Conv2d: 3-8 | [128, 64, 64] | 147,840 |
| MaxPool2d: 3-9 | [128, 32, 32] | – |
| Conv2d: 3-10 | [256, 32, 32] | 295,680 |
| Conv2d: 3-11 | [256, 32, 32] | 590,592 |
| SelfAttention: 3-12 | [256, 32, 32] | 263,424 |

The density map regression layers ($f$), detailed in Table 7, are designed to predict density maps from the extracted features. Specifically, it expands the channels of features by deconv operations and estimates the density. The output size is input-alike but only one channel, which is shown as resized 256×256 px. And the $f_c$ shares weight and architecture with $f$ for preparing partial results map for CM validation.

Table 7: Architecture of regression layers in BiAN.

| Layer (Type: Depth-Idx) | Output Shape | Parameters (#) |
|---|---|---|
| Deconv2d: 3-13 | [128, 64, 64] | 131,456 |
| Conv2d: 3-14 | [128, 64, 64] | 295,296 |
| Conv2d: 3-15 | [128, 64, 64] | 147,840 |
| Deconv2d: 3-16 | [64, 128, 128] | 32,960 |
| Conv2d: 3-17 | [64, 128, 128] | 73,920 |
| Conv2d: 3-18 | [64, 128, 128] | 37,056 |
| Deconv2d: 3-19 | [32, 256, 256] | 8,288 |
| Conv2d: 3-20 | [32, 256, 256] | 18,528 |
| Conv2d: 3-21 | [32, 256, 256] | 9,312 |
| Conv2d: 3-22 | [1, 256, 256] | 33 |

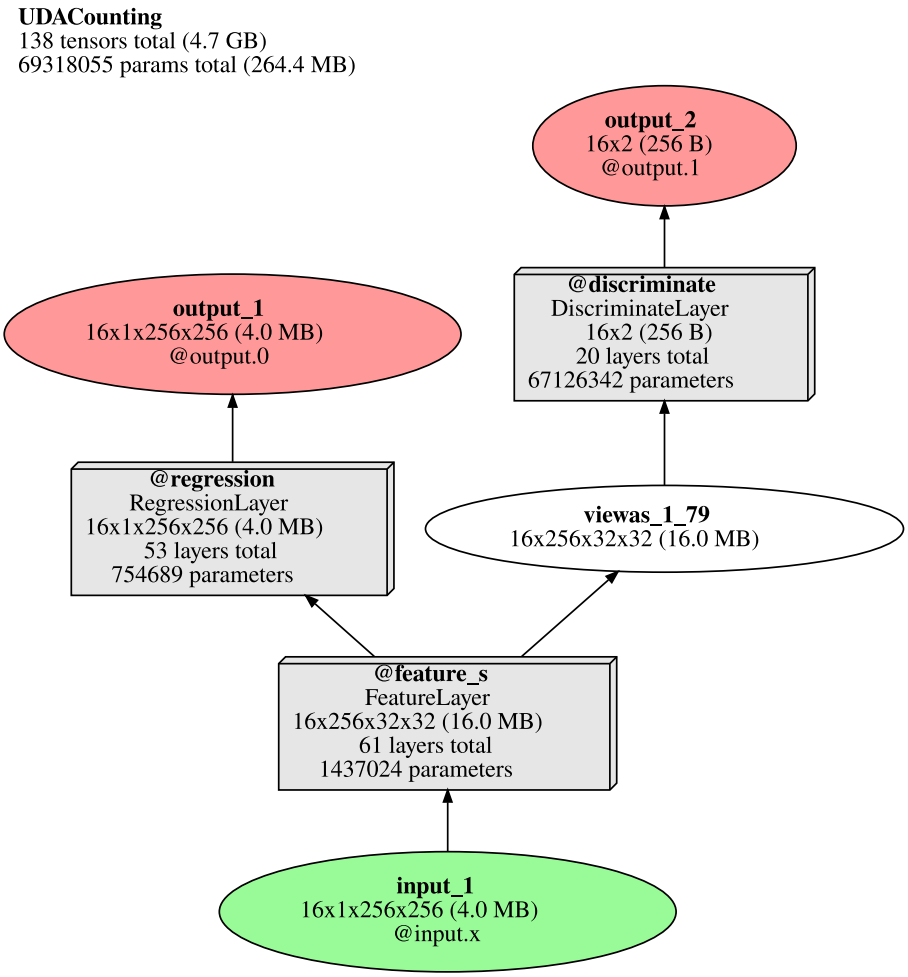


Figure 5: The network architecture visualization of BiAN. Note: The sample input is $16\times1\times256\times256$ px. Then estimated allocated memory is 4.7 GiB.

The domain discriminator ($f_d$), as described in Table 8, aims to align the domain distribution shift of features by broadcasting inverse gradient. The output is the binary label.

Table 8: Architecture of domain discriminate layers in BiAN.

| **Layer (Type: Depth-Idx)** | **Output Shape** | **Parameters (#)** |
|---|---|---|
| Linear2d: 3-23 | [256] | 67,109,632 |
| Linear2d: 3-24 | [64] | 16,576 |
| Dropout1d: 3-25 | [64] | – |
| Linear2d: 3-26 | [2] | 134 |
| Softmax: 3-27 | [2] | – |

### A.10 VISUALIZATION

In this section, we present the visual results of BiAN in the counting task experiments. As shown in Figure 7, we randomly select two samples from every cross-domain adaptation. In the visualization figure, we mark the inaccurate counts in the samples. The low-density samples can be counted in precise amounts, and the localization is also accurate. However, in microscopy cell images, cells of an overlapped or abnormal size are not fully recognized. The cell-alike objects (e.g. bubbles) easily distract the model recognition, especially in the DCC cell images. The conditional alignment mechanism enables BiAN to recognize distinguishing features of cells. As for the crowd counting task, human main characters are important cues to lead the model to marks. In contrast, the characters of hidden persons are easily missed targets. The results show that BiAN is able to retrieve the partial features of humans. It results in significant performance improvements. Overall, the visualization demonstrates the proposed model's recognition ability and learning of the visual representation of counting targets.

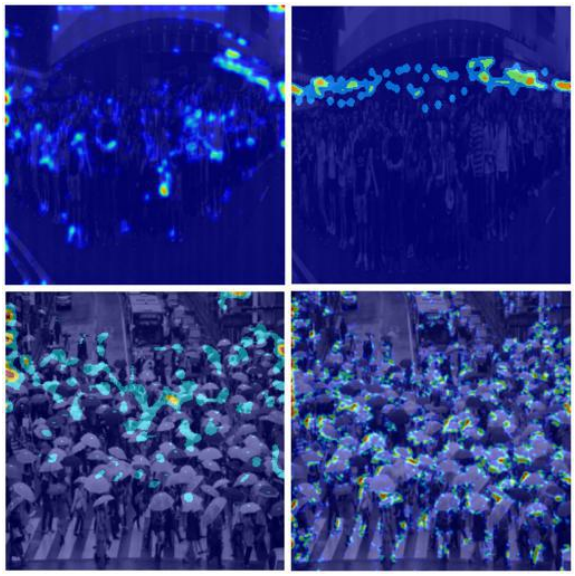

Figure 6: Density map visualization. Randomly selected two high-density samples from JHUCrowd++. The left ones are predictions, the right ones are labeled density maps.

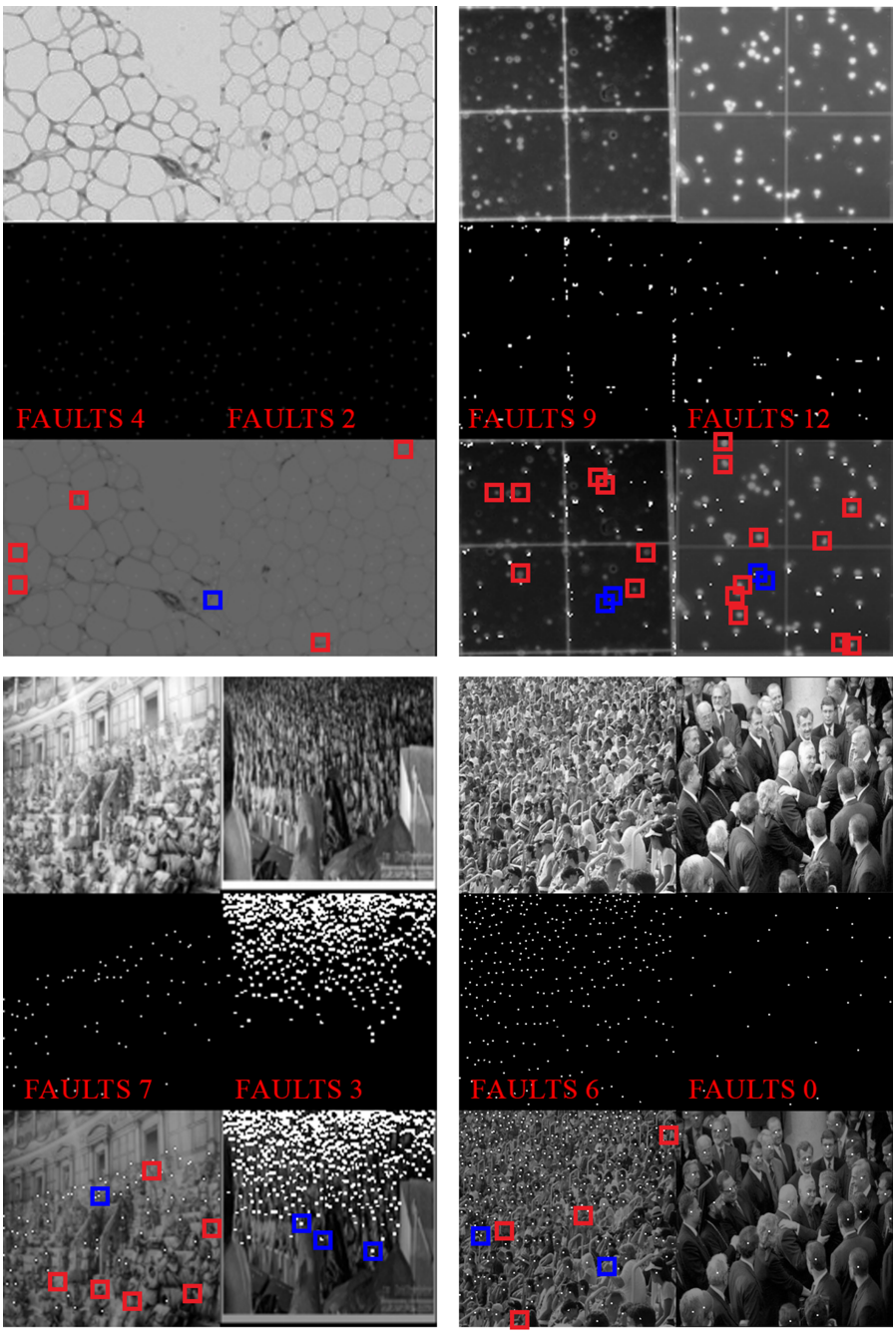


Figure 7: Dot map visualization. Randomly selected eight low-density samples from two adaptation tasks. From left to right, the samples are from ADI, DCC, UCF, SHB. The red mark indicates the miss count. The blue mark indicates the duplicated count.

### A.11 LIMITATIONS AND FUTURE WORK

This paper has several limitations that can be further investigated and improved. First, the lower bound of the aforementioned joint error is not the tightest (Zhao et al., 2019). It means the tightest lower bound of joint error might be lower than the loss bound mentioned above. However, this does not explicitly result in a performance drop. Second, the conditions are the label categories in BiAN, however Theorem 4 can fit more conditions. Regarding the designed model BiAN, we observed that there exists limited precision in recognizing and localizing, and counting minor objects. This aspect can be further improved in addition to the proposed CM. Nevertheless, our work emphasizes the importance of matching the conditions during the adaptation process and provides a promising direction for future research.